Experimental Study of a Vortex Generated at the Edge of a Channel with a Step

E.J. López-Sánchez, C.D. García-Molina, G. Ruiz-Chavarría and A. Medina

Abstract At the outlet of estuary-like systems, three vortices are formed: a dipole and a spanwise vortex. The spanwise vortex is formed due to the separation of the bottom boundary layer, just in front of the dipole. If a step occurs at the bottom in the channel output, a single vortex will be formed, the dipole becomes a part of a structure having a horseshoe shape. In a periodic driving flow, after a while this structure results in a dipole and a spanwise vortex. To study in laboratory this kind of vortices we made experiments in a system consisting of two domains connected by a channel in which the flow is induced by a periodic forcing. The channel layer depth is different with respect the depth in the two others domains. In order to investigate this system some measurements of velocity field using PIV were carried out in the vertical plane passing along the channel centerline. On the other hand, the detection of vortices composing the dipole was made with the synthetic Schlieren method. Vortices are low pressure regions, then they produce a deformation of the free surface which can be detected with this method. We observed that at the channel output a horseshoe vortex is formed by the flushing into the open domain. This structure remains for some time, after it decomposes in a dipole and a spanwise vortex. Finally all three vortices are destroyed.

1 Introduction

A large concentration of sand and other particles has been observed in front of coastal estuary-like systems (Albagnac et al. 2011), which may have many different interests, for instance in fishing or due to possible ship accidents. The aforesaid distribution is due to the presence of two counter rotating vortices. In the space between

E.J. López-Sánchez (✉) · C.D. García-Molina · G. Ruiz-Chavarría
Facultad de Ciencias, Universidad Nacional Autónoma de México
Ciudad Universitaria, 04510 Mexico, D.F., Mexico
e-mail: lsej@unam.mx

E.J. López-Sánchez · A. Medina
ESIME-Azcapotzalco, Instituto Politécnico Nacional, Av. de Las Granjas 682,
Azcapotzalco, Santa Catarina, 02250 Mexico, D.F., Mexico

J. Klapp et al. (eds.), *Recent Advances in Fluid Dynamics with Environmental Applications*, Environmental Science and Engineering, DOI 10.1007/978-3-319-27965-7_3

vortices a flow like a jet is produced, then the flow can carry particles for long distances compared with the channel width (Wells and Heijst 2003; Ruiz-Chavarria and Lopez-Sanchez 2016). Some previous works have been devoted to this kind of flow. For instance Nicolau del Roure et al. (2009) performed experiments to study a pair of counter rotating vortices formed in periodic flows in the shallow water approximation. They measured, among others, the position of the vortices, the maximum vorticity, the circulation and the effective diameter. For this purpose they used PIV to determine the velocity field in the surface and they measured geometrical properties through visualization. An important result is that the dipole produced in the first period behaves differently with respect to the dipoles produced in subsequent cycles. If the vortices escape channel influence, finally they are destroyed. Nicolau del Roure et al. (2009) associate this destruction to the friction on the bottom. However there exist other mechanisms, such as the appearance of instabilities (Crow 1970; Billant et al. 1999).

Apart from the dipole, a spanwise vortex has been recently reported (Lacaze et al. 2010; Albagnac et al. 2011). Its properties have been investigated both numerically and experimentally. This vortex appears as a consequence of the bottom boundary layer detachment. Albagnac (2010) made a comprehensive study of this structure when it is produced by the motion of two vertical flaps. She found that its shape resembles a horseshoe. In a periodic forced flow the shape of the spanwise vortex evolves in time (Lopez-Sanchez 2013; Lopez-Sanchez and Ruiz-Chavarria 2015). The motivation of this work is that in a periodic forced flow an accumulation of particles occurs inside the channel (Lopez-Sanchez and Ruiz-Chavarria 2014; Villamil Sapien et al. 2015), then the depth becomes non uniform. On the other hand, this kind of systems can be found in some coastal lagoons, during the rainy season. In such case, rain leads to an increase of the water level in the lagoon eventually producing the connection with to the sea.

In order to evaluate the effects of a channel with a depth lower than the remaining domains we have performed the following experiment. First, we induce a periodic driving flow. Then, we put a slug into the channel to reduce the depth by 25 and 50 %. Finally properties of vortices are investigated.

This paper is organized as follows: In Sect. 2 we present the theoretical framework and the dimensionless parameters governing the flow. In Sect. 3 the experimental setup is shown. The results of the PIV and synthetic Schlieren measurements are presented. Finally, in Sect. 5 conclusions are drawn.

2 Theoretical Framework

As result of periodicity of tides, water flow through the channel at estuary-like systems is periodic. To mimic this behavior we produce in laboratory a sinusoidal flow. The procedure to generate a variable flow rate $Q(t)$ is to partially submerge a solid block into the water. The displaced volume is:

$$V(t) = l \times a \times h(t) \tag{1}$$

where l is the block length, a is the width and $h(t) = h_0\,(1 - \cos(2\pi f\, t))$ is the instantaneous depth (the distance from free surface to the lower end of the block).

The flow rate is simply the time derivative of $V(t)$:

$$Q(t) = \frac{d\,V(t)}{d\,t} = 2\pi f \times l \times a \times h_0 \cos(2\pi f\, t) \tag{2}$$

Because water is incompressible and if we neglect changes in water level, $Q(t)$ is also the flow rate through the channel (Villamil Sapien et al. 2015). From the previous equation we found that the flow rate amplitude is:

$$Q_0 = 2\pi f \times l \times a \times h_0 \tag{3}$$

To determine the flow velocity into the channel we need to determine its cross area. This is $A = Hhn$, where H is the channel width, h is the layer depth in the two basins and n is the fraction of the water layer in the channel above the step. We have chosen two values of n, namely, $n = \frac{1}{2}$ and $n = \frac{3}{4}$. We can estimate the maximum velocity U in terms of the channel width H and the maximum flow rate Q_0 as

$$U = \frac{Q_0}{Hhn} \tag{4}$$

In this system two dimensionless numbers are relevant, the Strouhal and the Reynolds numbers. To define them we use the channel width H as the characteristic length, the representative velocity is that given in Eq. (4) and t is non dimensionalized with $\tau = H/U$. The Strouhal number is $S = \frac{U}{HT}$ while the Reynolds number is $Re = \frac{UH}{\nu}$. From these definitions, the dimensionless flow rate is:

$$Q^*(t^*) = Q_0^* \sin(2\pi S t^*) \tag{5}$$

From Eq. (4) the Reynolds number becomes:

$$Re = \frac{Q_0}{Hhn}\frac{H}{\nu} = \frac{Q_0}{hn\nu} \tag{6}$$

So, the Reynolds number does not depend on the channel width H.

On the other side, to calculate vorticity from velocity data, we use a second order centered finite differences schema, as follows:

$$\omega = \frac{\partial v}{\partial x} - \frac{\partial u}{\partial y} \approx \frac{v_{j+1} - v_{j-1}}{\Delta x} - \frac{u_{i+1} - u_{i-1}}{\Delta y} \tag{7}$$

Among other quantities we calculate vorticity and position of dipoles. To determine the position of vortices we use the idea of centroid. The last one is defined in terms of circulation. If we remember the definition of circulation (Dritschel 1986;

Landau and Liftshitz 1987), the vortex center (x_c, y_c) is:

$$\Gamma = \iint \omega \, dx \, dx \approx \sum \omega \, \Delta x \, \Delta y \tag{8}$$

$$x_c = \iint \frac{\omega \, x \, dx \, dy}{\Gamma} \tag{9}$$

$$y_c = \iint \frac{\omega \, y \, dx \, dy}{\Gamma} \tag{10}$$

To study the spanwise vortex we need to make a distinction between the vorticity created at the bottom and the vortex itself (even if vortex is feeded by wall vorticity). Before the appearance of the spanwise vortex, velocity field in the vicinity of the bottom is essentially horizontal. However, when vortex is present the vertical component of velocity is not negligible. A quantity well suited to determine the formation of the vortex is the vertical kinetic energy density (Lacaze et al. 2010):

$$E = \int v^2 \, ds \tag{11}$$

where integration extends over a vertical plane. This energy density quantifies the vertical movements which are not associated with the bottom boundary layer. Therefore, this quantity distinguishes between the vortex vorticity and boundary layer vorticity. It should be noted that for calculating the energy density, the portion near the vertical wall of the step has not been considered.

3 Experimental Setup

As can be seen in Fig. 1, we performed our experiments in a tank which consists of two basins connected by a channel. In our system, both basins have the same depth h, but in an attempt to get a more realistic model of estuary-like systems, the channel depth represents a fraction of h. We filled the tank with water up to get a uniform water layer of $h = 5.0$ cm. We have put a slug in the channel which reduces layer depth to 25 and 50 % of h.

To have different values of S and Re we have chosen an unique driving period $T = 12.5$ s and three different channel widths, namely, $H = 0.026$ m, $H = 0.04$ m and $H = 0.05$ m. The periodic water flow was induced by partially submerging a block having the following dimensions: $l = 0.577$ m, $a = 0.0149$ m. Otherwise the amplitude of its vertical motion is $h_0 = 0.015$ m.

Measurements were conducted in two ways: the study of the horizontal vorticity was made by PIV (Raffel et al. 1997; Meunier and Leweke 2003). The velocity field was measured in the vertical plane of symmetry. For this purpose we seed the water with glass coated silver spheres ($r = 5\,\mu$m) and we produce a vertical sheet with a solid state laser having a power of 1.6 W and emitting light at 532 nm. The images

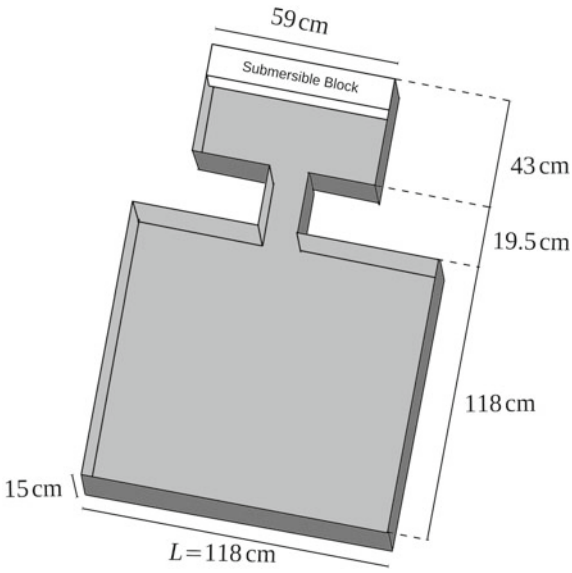

Fig. 1 Diagram of the experimental setup

we acquired with a high speed camera at a rate of 250 fps and covering an area of $0.10 \times 0.05\,\mathrm{m}^2$. The resolution of camera is 720×576 pixels and factor conversion between length and pixels is $\alpha = 4900\,\mathrm{px/m}$ Because we need to cover the region where vortex pass, the camera was put at two different locations. For those configurations we recorded two videos of three full periods each, these videos covered a distance of 0.14 m from the channel output with an overlap of 0.06 m. The first video covered from the channel output up to a distance of 0.10 m from it; and other one covered the interval from 0.04 to 0.14 m from the channel output.

To obtain properties of vertical vorticity we determined the free surface topography with the synthetic Schlieren method (Moisy et al. 2009). A vortex core is a low pressure region, then when it attains a free surface, variations of the water level are observed. As Synthetic Schlieren is a method for measuring the deformation in the water surface (Moisy et al. 2009), this technique is appropriate to characterize the formation and evolution of vortices attaining the free surface. To implement this method a dot pattern was placed at the bottom of the recipient. At a distance of 0.95 m above the water surface, we placed a video camera to record a dot pattern area of $L_1 \times L_2 = 0.206 \times 0.116\,\mathrm{m}^2$. With this configuration, the distance between the camera and the free surface is enough to avoid rays crossing (Moisy et al. 2009). To record image we take videos with a full high defintion camera, JVC Everio HD, modelGZ-HM845BE, at a rate 50 fps, with an image resolution of 1920×1080 pixels (Everio 2011). The factor conversion between length and pixels is 9300 pixel/m. Later, we have extracted individual images using software ffmpeg and finally they are processed with software DPIVsoft (Meunier et al. 2004).

4 Results

In this paper we present data of the velocity field in a vertical plane passing through the channel centerline. The images taken for PIV measurements have a resolution of 720×576 pixels and cover an area of $15.5\,\text{cm} \times 11.8\,\text{cm}$. Because the height of a frame is bigger than the water layer depth and also due to the size of the laser sheet, the frames were trimmed to a size of 400×260 pixels or 500×260. We have chosen cells of 32×32 pixels for the processing in the DPIV software.

On the other hand the evolution of the dipole was investigated with the synthetic Schlieren method. The images recorded have a size of 1920×1080 pixels and cover an area of $20.6\,\text{cm} \times 11.6\,\text{cm}^2$.

As we have mentioned above experiments were made for three different channel width: 2.6, 4 and 5 cm. In addition, two different layer depths into the channel were considered: $n = \frac{1}{2}$ and $n = \frac{3}{4}$. For the case $n = 1/2$; the transversal area of the channel is $A = 0.05 \times 0.03675 = 0.001225\,\text{m}^2$, and according to Eq. (4), $U = 0.106\,\text{m/s}$. For the case $n = 3/4$, the transversal area of the channel is $A = 0.05 \times 0.03675 = 0.0018375\,\text{m}^2$ and $U = 0.071\,\text{m/s}$. Given these quantities, the Reynolds and Strouhal numbers can be computed; these values are presented in the Table 1.

All the experimental configurations described in this article gave us similar results, so we have decided to present the most representative ones, the case with $n = 1/2$.

4.1 PIV Measurements

The fluid leaving the channel forms a single vortex. The two branches, which in other circumstances forms a dipole, now are connected near the bottom. The horizontal section of this structure initially is located near the step and after it moves and approaches the bottom. Later it goes away from the channel, the vortex is divided in a dipole and a clockwise vortex. Finally the latter is destroyed during the stage of negative flow rate at a distance of approximately of one time the channel width, whereas the dipole remains for more than one cycle.

Figure 2 shows a sequence of the velocity field in the symmetry plane for the $S = 0.0732$ (see Table 1). The horizontal section of vortex is produced just at the edge of the channel in the same manner as the two vertical branches, that is, because the

Table 1 Values of Reynolds and Strouhal numbers for all cases here studied

	$n = 1/2,\ \ Re = 2734$	$n = 3/4,\ \ Re = 1823$
$H = 0.05\,\text{m}$	$S = 0.0732$	$S = 0.1097$
$H = 0.04\,\text{m}$	$S = 0.0468$	$S = 0.0702$
$H = 0.026\,\text{m}$	$S = 0.0198$	$S = 0.0297$

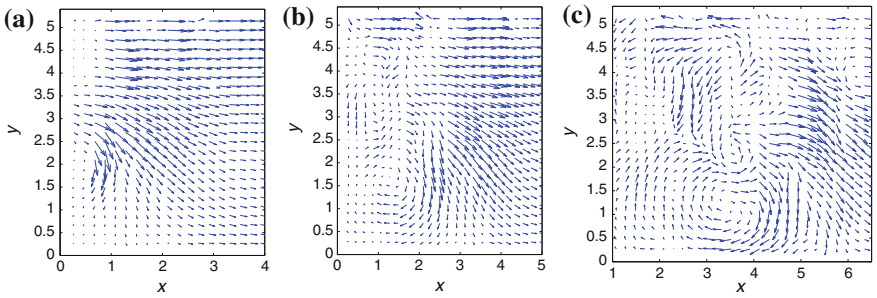

Fig. 2 Time evolution (as a function of the period T) of the velocity field in the vertical plane at the symmetry axis between 0 and 10 cm for $S = 0.0732$. **a** $t = 0.1143\,T$s. **b** $t = 0.2\,T$. **c** $t = 0.29\,T$

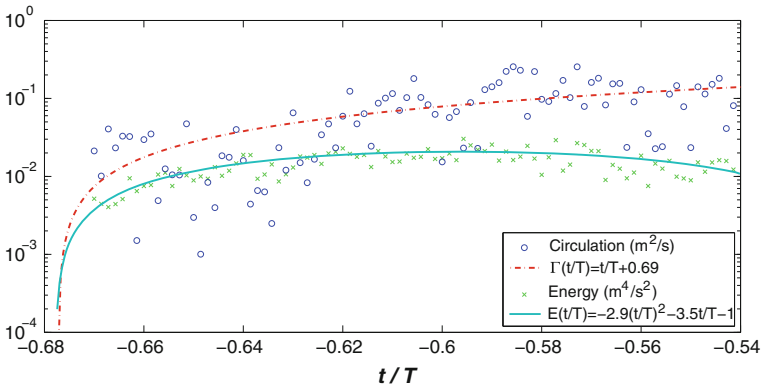

Fig. 3 Circulation and energy density at the vertical rectangular plane $x \in (0, 6)$ cm and $y \in (0, 2.5)$ cm, where the vortex is

boundary layer separation. According to our reference system, the vorticity is negative. In Fig. 2a the initial stage of the vortex formation can be observed. Figure 2b shows the vortex at a time close to that of maximum flow rate. Finally, in Fig. 2c we can see the transversal vortex at the bottom, and to a distance of $x \approx 3.5$ cm from the channel output. The size of vortex is larger than that shown in Fig. 2b.

In Fig. 3 we plot the circulation and the vertical kinetic energy versus time during the first half driving period. Initially circulation is zero because fluid is at rest. After it increases due to the addition of the vorticity created by the non slip condition in the channel's bottom. Circulation attains a local maximum and then decreases until the final dissipation of this section of the vortex. This reduction is related to the bottom friction and the fact that near the wall vorticity of opposite sign is created. On the other hand, the vertical energy density is an increasing function of time. It means that the vortex grows in size and also in intensity along the half period. The experimental data for Γ and E were fitted with a polynomial. In the first case we choose a cubic fit, whereas for E a quadratic one was made. Both curves are included, they are the dashed and the continuous lines respectively in the figure.

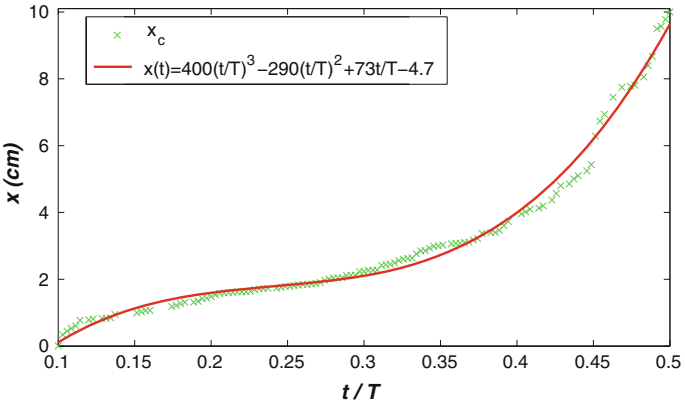

Fig. 4 Position of the horizontal section of vortex in the interval $x \in (0, 10)$ cm within a half period

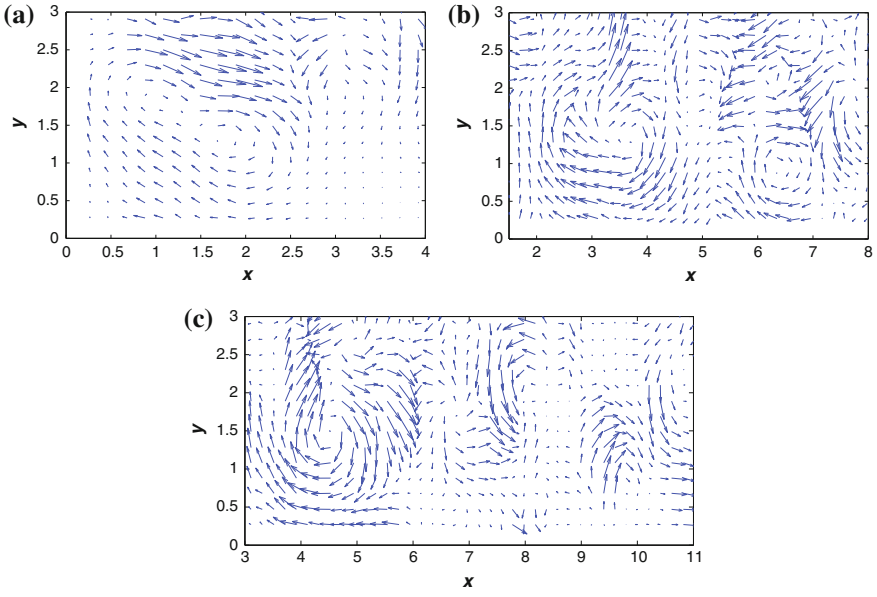

Fig. 5 Velocity field in the vertical plane at the symmetry axis during the second driving period. **a** At $t = 1.11\,T$ we observe an elongated vortex **b** $t = 1.23\,T$, two vortices are observed, one of them at $x \approx 3.5$ cm. $x \approx 6.5$ cm. **c** Velocity field at $t = 1.45\,T$

The vortex position was estimated based on the centroid calculation Eqs. (9) and (10). The center does not fall to the bottom completely (see Fig. 2c). At $t = 0.5\,T$ the vortex center is approximately to a distance of $h_{cent} \approx 1$ cm from the bottom. Based in data of centroids the distance traveled by the horizontal branch of the vortex is presented in Fig. 4. The data wera fitted with a cubic polynomial. Initially the speed

is small, $v \approx 0.3$ cm/s. After a while the vortex is accelerated and it reaches a velocity of $v \approx 3.5$ cm/s.

Figure 5 shows three snapshots of the velocity field over the second driving period. In Fig. 5a we see the velocity field at $t = 1.11\,T$. It is important to remark that flow properties are different when compared with the same stage at the first cycle. In particular the vortex now is elongated. The same behavior has been observed for other values of S an Re. After a while, at $t = 1.23\,T$, we can observe a velocity field indicating the presence of two vortices at $x \approx 3.5$ cm and $x \approx 6.5$ cm (see Fig. 5b). This behavior is presumably the result of the detachment of a fraction of the vorticity of the elengated vortex an to the bottom bounddary layer separation. Finally, in Fig. 5c both vortices have moved and they are at $x \approx 4.5$ and $x \approx 9.5$ respectively.

4.2 Dipole Properties

To study the dipole we use synthetic Schlieren method. The Fig. 6 shows the topography of the free surface at two different times. Vortex core in Fig. 6 coincides with free surface depression. The amplitude of depression is roughly proportional to vortex intensity. Figure 6a shows free surface deformation at $t = 0.5\,T$, that is, during the first cycle. While in Fig. 6b we show the free surface deformation at $t = 1.4\,T$, that is, in the subsequent period. Here we observe that at the first period, the depression amplitude is around a half of the depression amplitude for the successive cycles. Which is another expression that the vortex in the first cycle have differences with vortices produced in the subsequent cycles.

Figure 7 shows the deformation of the surface in two different cycles. In the first period Fig. 7a it can be observed a dipole leaving the channel. This dipole is the only one in the first cycle. In Fig. 7b we can observe the surface deformation at $t = 1.1\,T$. Apart of the main dipole created in each cycle (in Fig. 7b in the position $x = 4$ cm) we can see another depression at $x = 1$ cm, $y = -3$ cm corresponding to a secondary vortex formed after the main dipole.

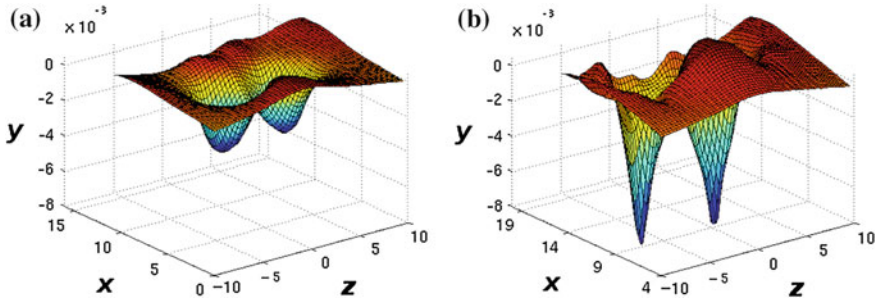

Fig. 6 Deformation of the water surface at two times. **a** $t = 0.5\,T$. **b** $t = 1.4\,T$

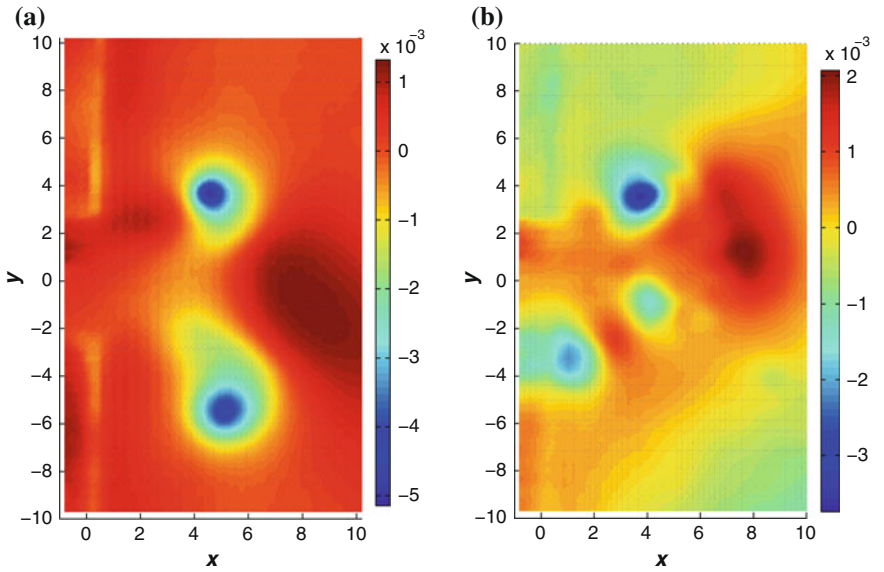

Fig. 7 Deformation of the water surface at two times. **a** $t = 0.23\,T$. **b** $t = 1.1\,T$

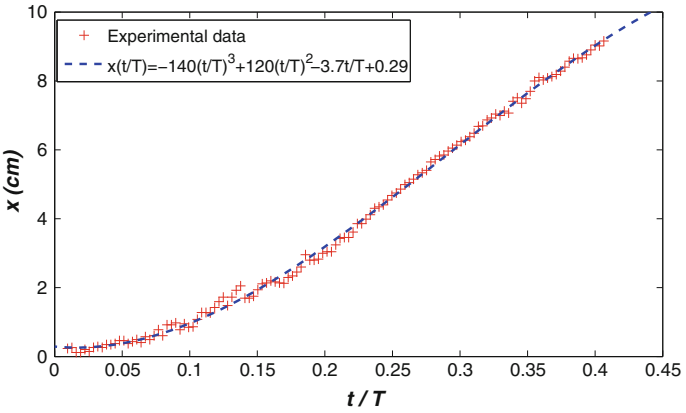

Fig. 8 Dipole displacement in function of t/T. These data was taken in an interval of 5 s. The displacement dipole velocity is $v_d \approx 0.8$ cm/s

Finally in Fig. 8 we present the position x of the dipole as a function of time. In the same figure a cubic fit is also included. At the end the vortex moves approximately with constant speed. At $t = 0.4\,T$ the dipole is in $x = 9$ cm, and its speed is 2.4 cm/s. By a linear regression, the mean dipole velocity in the range $t/T \in (0.1, 0.4)$ is 2 cm/s. According to data obtained with Schlieren method we observe that the dipole moves up to a distance of three times the channel width before its destruction.

5 Conclusions

In this paper we have presented some results of the flow between two basins connected by a channel. The channel and the basins have a different depth. The velocity field in a vertical plane and the deformation of the free surface were measured. These measurements provide information about vortices formed in front of the channel. First, the existence of an edge in the bottom at the channel output modifies the flow properties with respect of a system with constant depth. The adverse gradient pressure in the open domain leads to the formation of a horseshoe vortex. In other conditions only two counter rotating vortex are produced. In this case the two vortices are connected near the bottom, forming an unique structure. The further evolution is influenced by the bottom friction. For $t/T < 1/2$ the transverse section of the horseshoe vortex approaches the bottom. After the vortex splits in a dipole and a spanwise vortex. On the other side, during the stage of negative flow rate the streamwise vortex dissapears because the combined effect of bottom friction and the production of vorticity of opposite sign near the bottom.

As in the previous works in which bottom is constant (Lacaze et al. 2010; Albagnac 2010; Albagnac et al. 2011), a streamwise vortex appears in front of the dipole. It travels a distance of approximately three times the channel width before its destruction

Acknowledgments Authors acknowledge DGAPA-UNAM by support under project IN116312 (Vorticidad y ondas no lineales en fluidos). E. J. López-Sánchez thanks CONACYT and IPN.

References

Albagnac J (2010) Dynamique tridimensionnelle de dipoles tourbillonnaires en eau peu profonde. Thèse de doctorat, Université Paul Sabatier Toulouse III Institut de Mcanique des Fluides de Toulouse, France

Albagnac J, Lacaze L, Brancher P, Eiff O (2011) On the existence and evolution of a spanwise vortex in laminar shallow water dipoles. Phys Fluids 23:086601

Billant P, Brancher P, Chomaz JM (1999) Three dimensional stability of a vortex pair. Phys Fluids 11:2069-2077

Crow SC (1970) Stability theory for a pair of trailing vortices. AIAA J 8(12):2172

del Roure Nicolau F, Sokolofsky SA, Chang K (2009) Structure and evolution of tidal starting jet vortices at idealized barotropic inlets. J Geophys Res 114:C05024

Dritschel DG (1986) The nonlinear evolution of rotating configutations of uniform vorticity. J Fluid Mech 172:157–182

Everio JVC (2011) CAMCORDER Detailed User Guide. Victor Company of Japan website. http://manual3.jvckenwood.com/c1c/lyt2339-010sp/

Lacaze L, Brancher P, Eiff O, Labat L (2010) Experimental characterizat ion of the 3D dynamics of a laminar shallow vortex dipole. Exp Fluids 48:225–231

Landau LD, Liftshitz EM (1987) Fluid mechanics. Pergamon Press, Oxford, UK

Lopez-Sanchez E.J (2013) Vorticidad y transporte de partculas en un flujo peridico a la salida de un canal. PhD thesis. Facultad de Ciencias, UNAM, México

Lopez-Sanchez EJ, Ruiz-Chavarria G (2014) Transport of particles in a periodically forced flow. In: Experimental and computational fluid mechanics. Springer International Publishing, pp 271–278

Lopez-Sanchez EJ, Ruiz-Chavarria G (2015) Numerical simulation of the spanwise vortex in a periodic forced flow. submitted to: Experimental and computational fluid mechanics. Springer International Publishing

Meunier P, Leweke T (2003) Analysis and minimization of errors due to high gradients in Particle Image Velocimetry. Exp Fluids 35(5):408–421

Meunier P, Leweke T, Lebescond R, Van Aughem B, Wang C (2004) DPIVsoft. User guide. Institut de Recherche sur les Phnomnes Hors Equilibre. UMR 6594 CNRS / Universits Aix-Marseille I et II, Francia

Moisy F, Rabaud M, Salsac K (2009) A synthetic Schlieren method for the measurement of the topography of a liquid interface. Exp Fluids 46:10211036

Raffel M, Willert CE, Wereley ST, Kompenhans J (1997) Particle image velocimetry: a practical guide. Springer, Berlin

Ruiz-Chavarria G, Lopez-Sanchez EJ (2016) Formation of multiple dipoles in a periodic driving flow. submitted to: Phys. Fluids, AIP

Villamil Sapien P, Sánchez Calvo González I, Lopez-Sanchez EJ and Ruíz Chavarría G (2015) Erosion and deposition of particles in a periodic forced flow. In: Klapp J et al. (eds) Selected topics of computational and experimental fluid mechanics, environmental science and engineering. Springer International Publishing, pp 447–453

Wells MG, van Heijst G-JF (2003) A model of tidal flushing of an estuary by dipole formation. Dyn Atmos Oceans 37:223–244 (Elsevier)